

Variational material modeling of the transformation induced plasticity in polycrystalline steel

Johanna Waimann^{1*}, Stefanie Reese¹, and Philipp Junker²

¹ RWTH Aachen University, Institute of Applied Mechanics, Mies-van-der-Rohe-Straße 1, 52074 Aachen, Germany

² Ruhr-University Bochum, Institute of Continuum Mechanics, Universitätsstraße 150, 42801 Bochum, Germany

Abstract: The effect of transformation induced plasticity (TRIP) describes the coupling of plastic deformations and solid/solid phase transformations in steel. A result of this complex microstructural evolution is an improved ductility and strength of the so-called TRIP-steels, which is the reason for their attractiveness for industrial applications, e.g., in the automobile industry.

Modeling of the mentioned effects is an important aspect for enhancing the knowledge about the challenging processes that evolve in TRIP-steels. To this end, we present a variational material model that is based on the principle of the minimum of the dissipation potential. Considering kinematic hardening, the model describes the simultaneous evolution of an overall plastic strain and of the volume fractions of austenite and of several martensitic variants. Compared to our previous work [Waimann et al. \(2015\)](#), the polycrystalline structure is considered by an evolving orientation distribution function, which results in a much faster computation compared to our former investigations. Our analysis also covers the implementation into a finite element algorithm as well as the presentation of numerical results, which show the model's ability to give a first estimation for the complex material behavior.

Keywords: TRIP-steel, variational modeling, polycrystal, phase transformation, plasticity, kinematic hardening

1 Introduction

The eponymous effect of transformation induced plasticity (TRIP) in steel describes a simultaneous phase transformation and plastic deformation. The literature related to the particular modeling of the individual microstructural effects - the plastic deformation and the phase transformation - is huge. A good overview of plasticity is given in [Lubliner \(2008\)](#). Plasticity models based on variational concepts are exemplary given in [Han et al. \(1995\)](#); [Lubliner \(1984\)](#); [Mühlhaus and Alfantis \(1991\)](#) and for the case of crystal plasticity in, e.g., [Svendsen and Bargmann \(2010\)](#); [Hackl et al. \(2014\)](#); [Conti et al. \(2009\)](#). To mention but a few modeling concepts for martensitic phase transformations, we would like to refer to [Govindjee and Hall \(2000\)](#); [Auricchio and Petrini \(2004\)](#); [Govindjee and Miehe \(2001\)](#); [Turteltaub and Suiker \(2006b\)](#); [Babaei et al. \(2019\)](#). In the past, also, a lot of works have been related to the modeling of the special material behavior of TRIP-steels. Besides earlier works which couple the martensitic phase transformation with plastic deformation by, e.g., [Greenwood and Johnson \(1965\)](#), [Leblond et al. \(1986\)](#), [Leblond et al. \(1989\)](#), [Fischer \(1990\)](#). The model of [Levitas \(1998\)](#) also examined the martensitic transformation at interfaces and thus at discontinuities of the displacement field in an inelastic material. The model by [Olson and Cohen \(1975\)](#) is the basis for the later studies [Iwamoto and Tsuta \(2000, 2002\)](#): the martensitic transformation is driven by a shear band intersection and a stochastic ansatz is used for the formation of a nucleus. The extension [Iwamoto and Tsuta \(2000\)](#) accounts for a dependence on the austenitic grain size and furthermore, a high fracture toughness is examined in [Iwamoto and Tsuta \(2002\)](#). A study on the change of material properties related to hardening due to the TRIP effect based on [Iwamoto and Tsuta \(2000\)](#) is given in [Dan et al. \(2008\)](#). Another promising approach based on stochastic considerations is presented in [Ostwald et al. \(2011\)](#) for one-dimensional problems; its 3D-extension and finite-element-implementation is given in [Ostwald et al. \(2012\)](#). The models are based on the probabilistic approach for phase transformations by [Govindjee and Hall \(2000\)](#) which may not only be applied for modeling the TRIP effect, but also for shape memory alloys. Also the work [Bartel et al. \(2011\)](#) of the same group presents an energy relaxation based approach, which uses a classical J_2 -vonMises-type plasticity. In this work a special focus lies on the inheritance of the plastic strain. Another energetic approach to predict the transformation induced plasticity is presented in [Bhattacharyya and Weng \(1994\)](#), wherein the phase fractions evolve depending on the reduction of the Gibb's energy. [Fischer et al. \(2000\)](#) the TRIP-effect is experimentally and theoretically examined and a constitutive material model is presented. The works of [Suiker and Turteltaub \(2005\)](#), [Turteltaub and Suiker \(2006a\)](#) and [Tjahjanto et al. \(2007\)](#) are based on the idea of a critical driving force. Representing the basic model, in [Suiker and Turteltaub \(2005\)](#) the material is divided into a transforming and a stable ferritic part. In its extensions in [Turteltaub and Suiker \(2006a\)](#) and [Tjahjanto et al. \(2007\)](#), the influence of both the material parameters, which characterize the microstructure, and the crystal sizes are studied. A rather phenomenological approach but thus computationally very fast ansatz was presented in [Thibaud et al. \(2006\)](#), in which an evolution equation for the martensitic volume fraction is assumed which depends on the plastic strain rate.

In this work, we present a variational material model which is based on our previous approach presented in [Waimann et al.](#)

* E-mail address: johanna.waimann@ifam.rwth-aachen.de doi: [10.24352/UB.OVGU-2020-017](https://doi.org/10.24352/UB.OVGU-2020-017)

(2015). Using the principle of the minimum of the dissipation potential (PMDP), we derived coupled evolution equations for the plastic deformation and phase transformation. Now, we present a computationally improved model: instead of accounting for the polycrystalline character by discretizing the orientation distribution function using a large number of distinct orientations for which calculating the grain-wise phase transformation was necessary, we make use of an ansatz for an evolving orientation distribution function, given by Junker (2014). This approach takes into account the polycrystalline structure and thus different oriented grains of the examined material by Euler angles that parameterize the “effective” orientation of transforming grains. The material model is then equipped with evolution equations for the Euler angles. Although evolution equations for the volume fractions, the plastic strains, and the Euler angles have to be solved, the numerical effort is smaller by orders of magnitude as compared to the original ansatz with volume fractions and plastic strains for a large number of individually discretized grains as in Waimann et al. (2015).

In the first chapter, we introduce the variational concept and present the micromechanical model describing the TRIP effect. In the following section we show the results of a material point calculation with prescribed strain and a finite-element-simulation for a plate with a hole. Our article is completed by a conclusion and an outlook on further investigations.

2 Variational modeling of TRIP-steel

Our material model is based on the so-called principle of the minimum of the dissipation potential (PMDP) [cf. Carstensen et al. (2002); Hackl and Fischer (2008)] and it represents an extension of the model for phase transformation in shape memory alloys Hackl and Heinen (2008). As presented in Junker (2016), the PMDP represents a special case of the well-known Hamilton’s principle presented in Hamilton (1834, 1835) which allows to derive evolution equations that have a field function character. The variational concept is based on the idea of formulating a Lagrange function \mathcal{L} which includes the rate of the Helmholtz free energy ψ as well as a dissipation function \mathcal{D} . The energy ψ depends on primary variables, e.g., the symmetrized gradient of the displacement field $\nabla^{\text{sym}} \mathbf{u} = \frac{1}{2}(\nabla \mathbf{u} + \mathbf{u} \nabla) =: \boldsymbol{\varepsilon}$, indicating the strains, and/or the temperature θ , and a set of internal variables $\boldsymbol{\Lambda}$ which describe the microstructure. The dissipation function denotes the energy which dissipates due to the microstructural change and thus, depends at least on the rate of $\boldsymbol{\Lambda}$. Assuming that every material prefers a state of minimum energy, the minimization of the Lagrangean with respect to $\dot{\boldsymbol{\Lambda}}$ directly results in evolution equation for the internal variables. The minimization problem reads

$$\mathcal{L} = \dot{\psi}(\boldsymbol{\varepsilon}, \theta, \boldsymbol{\Lambda}) + \mathcal{D}(\dot{\boldsymbol{\Lambda}}) \rightarrow \min_{\dot{\boldsymbol{\Lambda}}} . \quad (1)$$

During the later minimization a further summand is added to the Lagrange function, which enables the consideration of the constraints to be observed. We will show this in the following sections.

2.1 Internal variables

To describe the microstructure of the polycrystalline TRIP-steel, we make use of four internal variables:

- the volume fractions of the austenite and the martensites $\boldsymbol{\lambda}$
- the plastic strain $\boldsymbol{\varepsilon}^p$
- the kinematic hardening variable $\boldsymbol{\alpha}^v$
- a set of Euler angles $\boldsymbol{\alpha} = \{\varphi, \vartheta, \omega\}$,

consequently: $\boldsymbol{\Lambda} = \{\boldsymbol{\lambda}, \boldsymbol{\varepsilon}^p, \boldsymbol{\alpha}^v, \boldsymbol{\alpha}\}$. The vector $\boldsymbol{\lambda}$ contains the individual phase fractions which are related to the transformation process: the austenitic ($i = 0$) and the n different martensitic ($1 \leq i \leq n$) phases. It has to fulfill the constraints of non-negativity and mass conservation. In contrast to our material models for shape memory alloys [cf. Waimann et al. (2019)], where the complete material is able to transform, we consider here that only a small amount of the material at the observed material point is able to show the phase transition between austenite and martensite. The rest of the material is ferritic or bainitic and has a fixed, time- and load-invariant volume fraction of λ_{BF} . Due to mass conservation, the sum of all evolving fractions must be equal to the volume fraction of the transforming area:

$$\sum_{i=0}^n \lambda_i = 1 - \lambda_{\text{BF}} , \quad (2)$$

see also the sketched material point in Figure 1. When the condition (2) is fulfilled for the initialization, it is sufficient to guarantee that the sum of changes of $\boldsymbol{\lambda}$ is zero. The two constraints, which are considered later in the model, thus read:

$$\lambda_i \geq 0 \quad \forall i , \quad \sum_{i=0}^n \dot{\lambda}_i = 0 . \quad (3)$$

The second and third internal variables, $\boldsymbol{\varepsilon}^p$ and $\boldsymbol{\alpha}^v$, account for the plastic deformation with kinematic hardening. We make the assumption that the formed dislocations which are related to the plastic strain are spatially fixed and do not move with the phase fronts. Therefore, the plastic strain state of the entire polycrystal is described by only one plastic strain tensor. We also want to point out that there are works in the literature which take into account a phase-wise plastic strain and thus, also consider the problem of inheritance of plastic strains [e.g., Bartel et al. (2011), Ammar et al. (2014)]. Following our - in a sense - more homogenized description and thus an averaged plastic strain and kinematic hardening variable comes along with a reduced

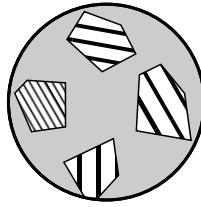


Fig. 1: Schematic transforming austenitic/martensitic (*white and black*) and non-transforming ferritic/bainitic (*grey*) regions at the material point.

computational effort. Furthermore, we have to consider the volume preservation during plastic deformation. Hence,

$$\dot{\boldsymbol{\varepsilon}}^p : \mathbf{I} = 0 \quad \text{and} \quad \dot{\boldsymbol{\alpha}}^v : \mathbf{I} = 0 \quad (4)$$

hold. Based on classical linear kinematic hardening rules [e.g., Lubliner (2008); Wriggers (2008)], we additionally fulfill:

$$\dot{\boldsymbol{\varepsilon}}^p = -\dot{\boldsymbol{\alpha}}^v. \quad (5)$$

Up to here, the current model substantially corresponds to our former model Waimann et al. (2015). However, one remarkable difference is the consideration of the polycrystalline structure. In our previous work Waimann et al. (2015), we assumed a coupled Voigt-Reuß-energy and modelled the austenitic/martensitic phase-transformation and plastic deformation for each particular grain. Thus, we used the volume fraction of transforming phase i in the grain j λ_i^j and the plastic strain in the grain j $\boldsymbol{\varepsilon}^{pj}$ as internal variables. To get rid of such a numerically expensive grain-wise computation of the internal variables, we are now calculating an averaged volume fraction of the austenitic and martensitic phases as well as an overall plastic strain for the whole material point. To this end, let us introduce the set of Euler angles $\boldsymbol{\alpha}$ which describes the averaged orientation of the transforming grains [see Junker (2014)]. The set of Euler angles allows us to take into account the orientation by use of a rotation tensor $\mathbf{Q} = \mathbf{Q}(\boldsymbol{\alpha})$. Thereby, we significantly decrease the numerical effort of the new model.

2.2 Helmholtz free energy

Using the internal variables defined in the last section, we can formulate our Helmholtz free energy, which describes the energy of the examined TRIP-steel. We use a Reuss energy bound and thus, assume a constant stress at the material point:

$$\psi = \frac{1}{2} (\boldsymbol{\varepsilon} - \bar{\boldsymbol{\eta}}_R - \boldsymbol{\varepsilon}^p) : \bar{\mathbb{E}} : (\boldsymbol{\varepsilon} - \bar{\boldsymbol{\eta}}_R - \boldsymbol{\varepsilon}^p) + \bar{c} + \frac{1}{3} \mathbf{a}^v : \bar{\mathbb{H}} : \mathbf{a}^v. \quad (6)$$

In Equation (6), the variable $\boldsymbol{\varepsilon}$ is the total strain. As a result of the applied Reuss bound, the effective quantities of the phase-wise transformation strain $\boldsymbol{\eta}_i$, stiffness tensor \mathbb{E}_i , hardening tensor \mathbb{H}_i , and the caloric energy c_i can be calculated by

$$\begin{aligned} \bar{\boldsymbol{\eta}}_R &= \mathbf{Q}^T(\boldsymbol{\alpha}) \cdot \sum_{i=0}^n \lambda_i \boldsymbol{\eta}_i \cdot \mathbf{Q}(\boldsymbol{\alpha}) & \bar{c} &= \sum_{i=0}^n \lambda_i c_i \\ \bar{\mathbb{E}} &= \left(\sum_{i=0}^n \lambda_i \mathbb{E}_i^{-1} + \lambda_{\text{BF}} \mathbb{E}_{\text{BF}}^{-1} \right)^{-1} & \bar{\mathbb{H}} &= \left(\sum_{i=0}^n \lambda_i \mathbb{H}_i^{-1} + \lambda_{\text{BF}} \mathbb{H}_{\text{BF}}^{-1} \right)^{-1}. \end{aligned} \quad (7)$$

Assuming isotropy for stiffness and hardening tensor, only the transformation strain is rotated in the orientation given by the set of Euler angles. Of course, other (and less) assumptions on the stress in the material point are possible. However, such much more sophisticated mixture energies stand in contrast to our goal of presenting a material law which can be implemented using a computationally more efficient algorithm compared to our previous model Waimann et al. (2015). We therefore stick to the rather simplified assumption of a constant stress in all crystallographic phases.

For the use of the Lagrange function (1), we need to calculate the rate of the Helmholtz free energy. Therefore, we are introducing the thermodynamical driving forces

$$\begin{aligned} P_{Ti} &= -\frac{\partial \Psi}{\partial \lambda_i} = \mathbf{Q}^T \cdot \boldsymbol{\eta}_i \cdot \mathbf{Q} : \boldsymbol{\sigma} + \frac{1}{2} \boldsymbol{\sigma} : (\mathbb{E}_i)^{-1} : \boldsymbol{\sigma} - c_i + \frac{1}{3} \mathbf{a}^v : \bar{\mathbb{H}} : \mathbb{H}_i^{-1} : \bar{\mathbb{H}} : \mathbf{a}^v \\ P_P &= -\frac{\partial \Psi}{\partial \boldsymbol{\varepsilon}^p} = \boldsymbol{\sigma} \\ P_V &= -\frac{\partial \Psi}{\partial \mathbf{a}^v} = \frac{2}{3} \bar{\mathbb{H}} : \mathbf{a}^v \\ P_R &= \{P_\varphi, P_\theta, P_\omega\}^T = -\frac{\partial \Psi}{\partial \boldsymbol{\alpha}} = 2\bar{\boldsymbol{\eta}} \cdot \mathbf{Q} \cdot \boldsymbol{\sigma} : \frac{\partial \mathbf{Q}}{\partial \boldsymbol{\alpha}}, \end{aligned} \quad (8)$$

whereby σ describes the stress tensor, which is calculated by

$$\sigma = \mathbb{E} : (\varepsilon - \bar{\eta}_R - \varepsilon^P) . \quad (9)$$

By use of the chain rule, we can calculate the rate of the Helmholtz free energy by

$$\dot{\psi} = -P_T \cdot \dot{\lambda} - P_P : \dot{\varepsilon}^P - P_V : \dot{a}^V - P_R \cdot \dot{\alpha} . \quad (10)$$

2.3 Dissipation function

As mentioned before, the dissipation function describes the energy which is dissipated during microstructural evolution. For the simultaneous phase transformation and plastic deformation, we use a coupled dissipation function based on [Waimann et al. \(2016\)](#) which will result in rate-independent evolution equations. For the change of the Euler angles, we use the approach given by [Junker \(2014\)](#) which is homogeneous of second order and will result in evolution equations of viscous type. The dissipation function reads

$$\mathcal{D} = r_T \sqrt{\sum_{i=0}^n \dot{\lambda}_i^2 + a^2 \dot{\varepsilon}^P : \dot{\varepsilon}^P} + \frac{\sqrt{2} r_R}{2} (\dot{\varphi}^2 + \dot{\vartheta}^2 + 2\dot{\varphi}\dot{\omega} \cos \vartheta + \dot{\omega}^2) , \quad (11)$$

whereby r_T is the dissipation parameter which describes the amount of energy necessary for the microstructural change and r_R is the viscosity parameter for the dynamic orientation distribution function. The parameter a is a coupling factor which accounts for the different amount of energy for the plastic deformation compared to the transformation. It is calculated in dependence of the plastic yield limit Y_0 by $a = Y_0/r_T$. Considering now a pure plastic deformation and thus $\dot{\lambda} = \mathbf{0}$, the dissipation function reduces to its classical form used for plasticity. Note that the part for the rates of the Euler angles ensures objectivity.

2.4 Lagrange function, evolution equations and related yield function

Inserting now the rate of the Helmholtz free energy (10) and the dissipation function (11) into the Lagrangean (1) results in the minimization problem

$$\begin{aligned} \mathcal{L} = & -P_T \cdot \dot{\lambda} - (P_P - P_V) : \dot{\varepsilon}^P - P_R \cdot \dot{\alpha} + r_T \sqrt{\sum_{i=0}^n \dot{\lambda}_i^2 + a^2 \dot{\varepsilon}^P : \dot{\varepsilon}^P} + \frac{\sqrt{2} r_R}{2} (\dot{\varphi}^2 + \dot{\vartheta}^2 + 2\dot{\varphi}\dot{\omega} \cos \vartheta + \dot{\omega}^2) \\ & + \kappa_T \sum_{i=0}^n \dot{\lambda}_i - \sum_{i=0}^n \gamma_{Ti} \dot{\lambda}_i + \kappa_P \dot{\varepsilon}^P : \mathbf{I} \quad \rightarrow \quad \min_{\dot{\alpha}, \dot{\lambda}, \dot{\varepsilon}^P} , \end{aligned} \quad (12)$$

whereby the constraints (3) and (4) are considered by the Lagrange parameters κ_T and κ_P and the Kuhn-Tucker parameter γ_T . The fourth constraint (5) is directly inserted.

By solving the minimization problem, we can now directly calculate the evolution equations for the internal variables. The viscous evolution equations for the three Euler angles read

$$\begin{aligned} \dot{\varphi} &= \frac{1}{\sqrt{2} r_R} \frac{1}{1 - \cos^2 \vartheta} (P_\varphi - P_\omega \cos \vartheta) \\ \dot{\vartheta} &= \frac{1}{\sqrt{2} r_R} P_\vartheta \\ \dot{\omega} &= \frac{1}{\sqrt{2} r_R} \frac{1}{1 - \cos^2 \vartheta} (P_\omega - P_\varphi \cos \vartheta) . \end{aligned} \quad (13)$$

The rate-independent evolution equations for the volume fractions and the plastic strain have the form

$$\begin{aligned} \dot{\lambda}_i &= \beta \operatorname{dev}_{\mathcal{A}} P_{Ti} \quad \forall i \in \mathcal{A} \\ \dot{\varepsilon}^P &= -\dot{a}^V = \frac{\beta}{a^2} \operatorname{dev} (P_P - P_V) \end{aligned} \quad (14)$$

with the active and the plastic deviator

$$\operatorname{dev}_{\mathcal{A}} P_{Ti} = P_{Ti} - \frac{1}{n_{\mathcal{A}}} \sum_{k \in \mathcal{A}} P_{Tk} \quad (15)$$

$$\operatorname{dev} (P_P - P_V) = (P_P - P_V) - \frac{1}{3} ((P_P - P_V) : \mathbf{I}) \mathbf{I} . \quad (16)$$

Introducing the set of $n_{\mathcal{A}}$ active phases $\mathcal{A} = \{i | \lambda_i > 0\} \cup \{i | \lambda_i = 0 \wedge \dot{\lambda}_i > 0\}$, the active deviator compares the driving force of a single phase with the averaged driving force of the active phases. The parameter β in (14) is called consistency parameter. It is a scalar function $\beta = \sqrt{\sum_{i=0}^n \dot{\lambda}_i^2 + a^2 \dot{\varepsilon}^P : \dot{\varepsilon}^P} / r_T$, which couples the evolution equations of the simultaneous phase transformation

and plastic deformation. For closing the system of equations, we apply a Legendre transformation of the dissipation function for the simultaneous processes

$$\mathcal{D}_T^* = \sup_{\lambda, \varepsilon^p} \left\{ \text{dev}_{\mathcal{A}} \mathbf{P}_T \cdot \dot{\lambda} + \text{dev}(\mathbf{P}_P - \mathbf{P}_V) : \dot{\varepsilon}^p - \mathcal{D}_T \Big|_{\mathcal{A}} \right\}, \quad (17)$$

which directly results in the yield function

$$\Phi_T = \text{dev}_{\mathcal{A}} \mathbf{P}_T \cdot \text{dev}_{\mathcal{A}} \mathbf{P}_T + \frac{1}{a^2} \text{dev}(\mathbf{P}_P - \mathbf{P}_V) : \text{dev}(\mathbf{P}_P - \mathbf{P}_V) - r_T^2 \quad (18)$$

and the Karush-Kuhn-Tucker conditions

$$\beta \geq 0, \quad \Phi_T \leq 0 \quad \beta \Phi_T = 0, \quad (19)$$

which enable us to quantify β . With the evolution equations (14) and (13), the yield function (18) and the Karush-Kuhn-Tucker conditions (19) our model is set. Note that the coupled approach for the dissipation function in (11) gives one single yield function that indicates the onset and offset of the coupled evolution of volume fractions, plastic strains, and back stress. The evolution of the “effective” orientation, indicated by the Euler angles, is not constrained and is determined solely by the driving forces $\mathbf{P}_R \neq \mathbf{0}$. This case is present as soon as martensitic variants are present, i.e., $\lambda_{i>0} \neq 0$ for any variant i .

3 Numerical results

In the following subsections, we used the material parameters presented in Ostwald et al. (2011) and thus six different martensitic phases with the transformation strains (in Voigt notation):

$$\begin{aligned} \boldsymbol{\eta}_1 = -\boldsymbol{\eta}_4 &= \hat{\eta} \{1, -\hat{\nu}, -\hat{\nu}, 0, 0, 0\}^T \\ \boldsymbol{\eta}_2 = -\boldsymbol{\eta}_5 &= \hat{\eta} \{-\hat{\nu}, 1, -\hat{\nu}, 0, 0, 0\}^T \\ \boldsymbol{\eta}_3 = -\boldsymbol{\eta}_6 &= \hat{\eta} \{-\hat{\nu}, -\hat{\nu}, 1, 0, 0, 0\}^T \end{aligned} \quad (20)$$

with $\hat{\nu} = 0.3$ [-] and $\hat{\eta} = 0.04$ [-]. We choose the austenite as the reference phase for the transforming part of the material. Therefore, the transformation strain of the austenite is zero. In addition, we also set the transformation strain of the bainitic/ferritic phases to zero and interpret the two phases as the reference phases for the non-transforming part of the material. However, the constant phase composition leads to a constant energy contribution which has no influence on the performed minimization. For the stiffness tensors of all the individual phases, we choose an elasticity modulus of 160 GPa and a Poisson’s ratio of 0.3 [-]. The hardening tensor is for the austenitic phase $\mathbb{H}_0 = \mathbb{E}/4$ and for the other phases $\mathbb{H}_{i>0} = \mathbb{H}_{\text{BF}} = \mathbb{E}/12$. We neglect any temperature dependence, i.e. we set the caloric energy $c_i = 0$. The plastic yield limit is chosen to be $Y_0 = 1.00$ GPa and the non-transforming volume fraction $\lambda_{\text{BF}} = 0.8$ [-]. Additionally, the initial set of Euler angles is randomly generated: $\boldsymbol{\alpha}_0 = \{2.6260, 1.8406, 5.9814\}$ [-].

For the implementation of our problem, we choose a broken Taylor series for the discretization of the stress and the internal variables, see also Junker and Hempel (2017):

$$\boldsymbol{\Lambda}^{n+1} \approx \boldsymbol{\Lambda}^n + \left. \frac{\partial \boldsymbol{\Lambda}}{\partial t} \right|^n \Delta t. \quad (21)$$

Therein, $\boldsymbol{\Lambda}$ is a general discretized variable, n is the former and $n+1$ the current load step. The partial derivative $\left. \frac{\partial \boldsymbol{\Lambda}}{\partial t} \right|^n$ is the rate of the individual quantity at the previous load step. For the update of the internal variables this exemplary means

$$\lambda^{n+1} = \lambda^n + \left. \frac{\partial \lambda}{\partial t} \right|^n. \quad (22)$$

The update of the volume fraction is thus performed using the already calculated, and thus fixed, quantities of the previous step. Applying the explicit scheme also on the stress evolution

$$\boldsymbol{\sigma}^{n+1} = \boldsymbol{\sigma}^n + \left. \frac{\partial \boldsymbol{\sigma}}{\partial \boldsymbol{\varepsilon}} \right|^n : (\boldsymbol{\varepsilon}^{n+1} - \boldsymbol{\varepsilon}^n) + \left. \frac{\partial \boldsymbol{\sigma}}{\partial \lambda} \right|^n : (\lambda^{n+1} - \lambda^n) + \left. \frac{\partial \boldsymbol{\sigma}}{\partial \boldsymbol{\varepsilon}^p} \right|^n : (\boldsymbol{\varepsilon}^{p,n+1} - \boldsymbol{\varepsilon}^{p,n}) + \left. \frac{\partial \boldsymbol{\sigma}}{\partial \boldsymbol{\alpha}} \right|^n : (\boldsymbol{\alpha}^{n+1} - \boldsymbol{\alpha}^n) \quad (23)$$

results in the material tangent

$$\left. \frac{\partial \boldsymbol{\sigma}}{\partial \boldsymbol{\varepsilon}} \right|^n = \bar{\mathbb{E}}|^n \quad (24)$$

for the performed implementation in a finite element setting. The explicit scheme results in a very stable and robust algorithm which can be easily implemented.

3.1 Material point level

In our first simulation, we use a step-wise loading in form of a prescribed strain tensor (in Voigt notation):

$$\boldsymbol{\varepsilon} = \tilde{\varepsilon}\{1, -0.45, -0.45, 0, 0, 0\}^T \quad (25)$$

with $\tilde{\varepsilon} \in [-0.03, 0.03]$. The results of the tension/compression cycle are presented in Figure 2. We choose the dissipation parameter and the time-dependent discretized viscous parameter to be $r_T = 0.05$ GPa and $\Delta t_R = \Delta t / (\sqrt{2}r_R) = 0.01$ 1/GPa, respectively.

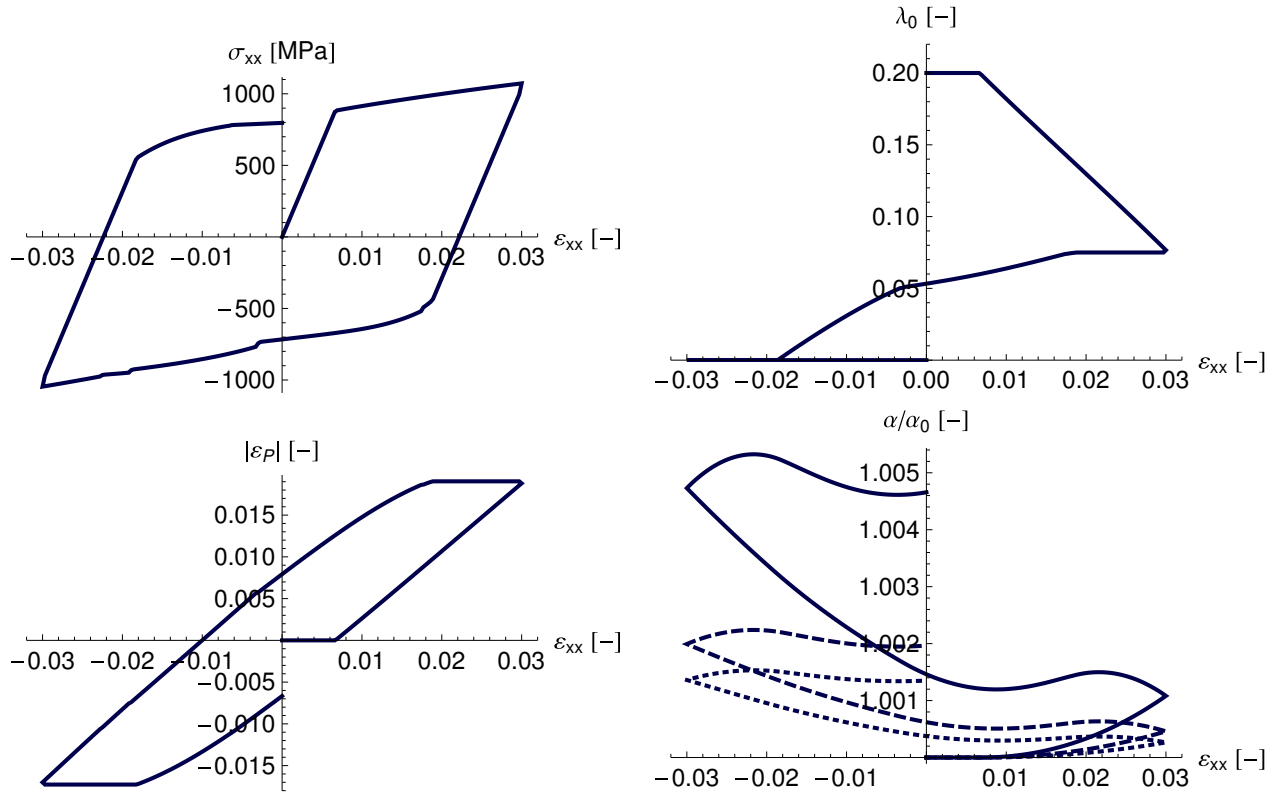


Fig. 2: Material point calculation: stress/strain diagram (*upper left*), austenitic volume fraction (*upper right*), norm of the plastic strain (*lower left*), relative change of the Euler angles (*lower right*).

As can be seen in the stress/strain diagram in Figure 2 (*upper left*), the material behaves linear elastic until reaching a critical stress, where the transformation and, simultaneously, the plastic deformation is initiated: the originally austenitic material transforms into martensite, see Figure 2 (*upper right*). Unloading leads again to a linear relation between stress and strain, until the transform starts again and the material transforms into the martensitic variants which are energetically favored for the unloading and afterwards compression. Unloading from the compressed state, leads again to a linear relation and a following transformation. After the load cycle, the material is not austenitic again. As can be seen in [Junker and Hempel \(2017\)](#), this is an effect of the plastic deformation within the model and reflects the experimentally observed behavior. Due to the coupled evolution equations, the transformation is accompanied by the evolution of the plastic strain, see Figure 2 (*lower left*). The relative change of the Euler angles in Figure 2 (*lower right*) show a permanent update of the orientation. Summarily, the variational model is able to qualitatively show the experimentally observed material behavior.

In Figure 3, the calculation is compared with results of the former model which is presented in [Waimann et al. \(2015\)](#). We used 100 randomly oriented grains for the grain-wise calculations of the polycrystalline material. The calculation time of the previous model [Waimann et al. \(2015\)](#) is 2.87042 s. The approach presented in this work and based on [Junker \(2014\)](#) needs only $1.56001 \cdot 10^{-2}$ s. The outstanding speed-up factor of 184, show the high improvement of the approach's efficiency by the dynamically evolving orientation distribution function. Nevertheless, although the plateau stress are in good accordance, the stress/strain curve shows a smoother initiation of the transformations, which results in a smooth transition between the elastic part and the stress plateaus. The reason for that is that some of the 100 grains start to transform earlier than others. Both models show a good first estimation for the expected material behavior and a good qualitative accordance to simulations performed, e.g., by [Ostwald et al. \(2012\)](#). However, an experimental comparison is necessary to further quantitatively examine the two modeling approaches.

3.2 Finite element simulation of a a plate with a hole

For our finite element simulation, we implemented an explicit solution scheme for the used internal variables, see [Junker and Hempel \(2017\)](#); [Waimann et al. \(2019\)](#). The boundary value problem of the loaded plate with a hole is presented in Figure 4 (left). The resulting force/displacement diagram of the applied tension/compression cycle is presented in Figure 4 (right). This global structure reaction shows similarities to the local behavior at the material point observed in the last section. The austenitic volume fraction as well as the absolute plastic deformation and the xx -component of the plastic strain are presented in Figures 5, 6 and 7, which show the simultaneous evolution of the coupled internal variables. Whereby the first and third plateaus in the force/displacement diagram are a result of the transformation from austenite to martensite, the major cause of the second plateau is a transformation between the martensitic variants. Finally, we showed that the implemented finite element algorithm using the explicit scheme is able to show the simultaneous microstructural evolutions, whereby a comparison with experiments is still pending.

4 Conclusion and outlook

We presented a variational material model, which is able to show a first estimation for the simultaneous plastic deformation and phase transformation in TRIP-steels. Compared to our previous model [Waimann et al. \(2015\)](#), we improved the computational effort by introducing an evolving orientation distribution function. The presented simulations for the material point level and a finite element calculation show the expected macroscopic behavior and are in good accordance with simulations by [Ostwald et al. \(2012\)](#). However, no experimental comparison and validation is done so far. Our next step is a more detailed examination of our model: by use of more simulations and an experimental validation, we will investigate the applicability of our model and calibrate the material parameters. In addition, the two different approaches for the polycrystalline structure - a grain-wise computation of the microstructural change presented in [Waimann et al. \(2015\)](#) and the here presented use of a dynamically evolving orientation distribution function - need a detailed examination and comparison based on experiments.

Acknowledgements We gratefully acknowledge the financial support of the Subproject M05 of the Transregional Collaborative Research Center SFB/TRR 136 by the German Science Foundation (DFG).

References

- K. Ammar, B. Appolaire, S. Forest, M. Cottura, Y. Le Bouar, and A. Finel. Modelling inheritance of plastic deformation during migration of phase boundaries using a phase field method. *Meccanica*, 49(11):2699–2717, 2014.
- F. Auricchio and L. Petrini. A three-dimensional model describing stress-temperature induced solid phase transformations: solution algorithm and boundary value problems. *International journal for numerical methods in engineering*, 61(6):807–836, 2004.
- H. Babaei, A. Basak, and V. I. Levitas. Algorithmic aspects and finite element solutions for advanced phase field approach to martensitic phase transformation under large strains. *Computational Mechanics*, pages 1–21, 2019.
- T. Bartel, A. Menzel, and B. Svendsen. Thermodynamic and relaxation-based modeling of the interaction between martensitic phase transformations and plasticity. *Journal of the Mechanics and Physics of Solids*, 59(5):1004–1019, 2011.
- A. Bhattacharyya and G. J. Weng. An energy criterion for the stress-induced martensitic transformation in a ductile system. *Journal of the Mechanics and Physics of Solids*, 42(11):1699–1724, 1994.
- C. Carstensen, K. Hackl, and A. Mielke. Non-convex potentials and microstructures in finite-strain plasticity. *Proceedings of the Royal Society of London. Series A: Mathematical, Physical and Engineering Sciences*, 458(2018):299–317, 2002.
- S. Conti, G. Dolzmann, and C. Klust. Relaxation of a class of variational models in crystal plasticity. *Proceedings of the Royal Society A: Mathematical, Physical and Engineering Sciences*, 465(2106):1735–1742, 2009.
- W. J. Dan, S. H. Li, W. G. Zhang, and Z. Q. Lin. The effect of strain-induced martensitic transformation on mechanical properties of TRIP steel. *Materials & Design*, 29(3):604–612, 2008.

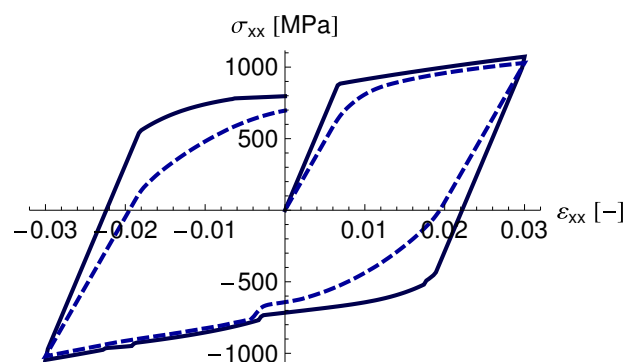


Fig. 3: Comparison of resulting stress/strain diagram of previous model (dashed) and current model.

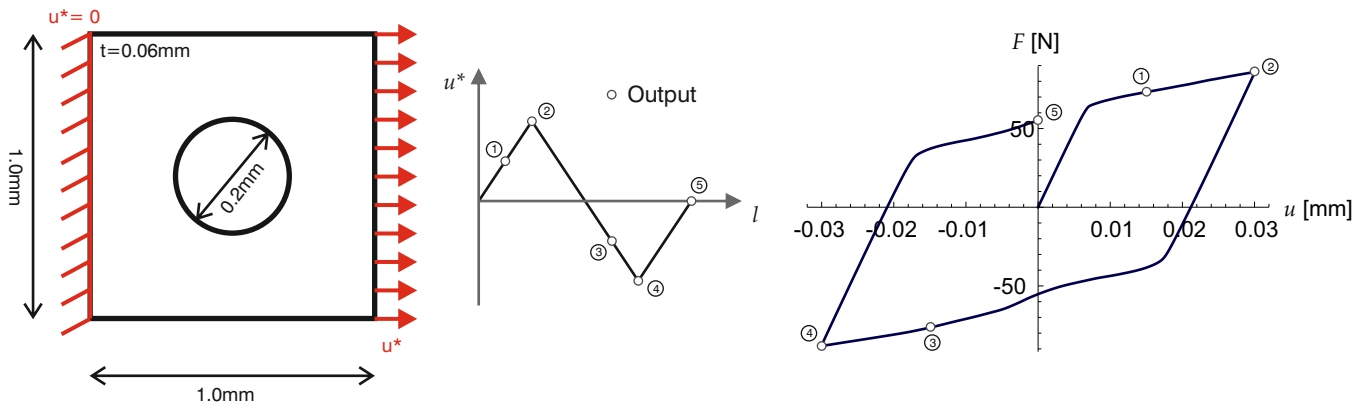


Fig. 4: Plate with a hole: boundary value problem (left), force/displacement diagram (right).

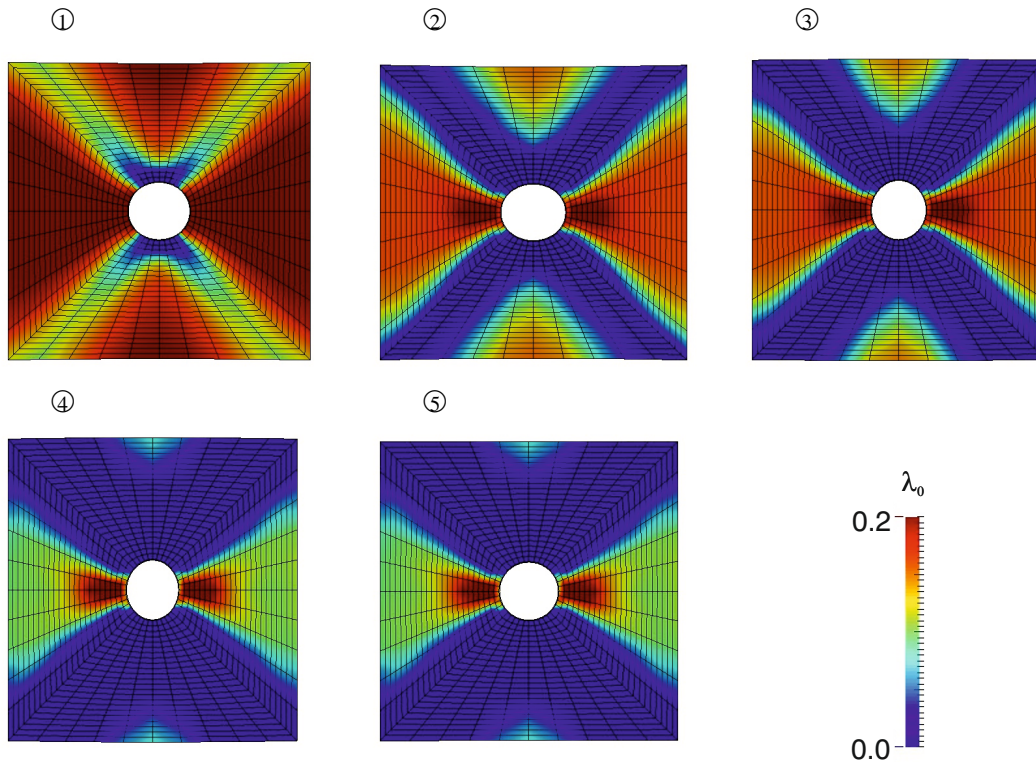


Fig. 5: Plate with a hole: austenitic volume fraction.

F. D. Fischer. A micromechanical model for transformation plasticity in steels. *Acta Metallurgica et Materialia*, 38(8):1535–1546, 1990.

F. D. Fischer, G. Reisner, E. Werner, K. Tanaka, G. Cailletaud, and T. Antretter. A new view on transformation induced plasticity (TRIP). *International Journal of Plasticity*, 16(7):723–748, 2000.

S. Govindjee and G. J. Hall. A computational model for shape memory alloys. *International Journal of Solids and Structures*, 37(5):735–760, 2000.

S. Govindjee and C. Miehe. A multi-variant martensitic phase transformation model: formulation and numerical implementation. *Computer Methods in Applied Mechanics and Engineering*, 191(3-5):215–238, 2001.

G. W. Greenwood and R. H. Johnson. The deformation of metals under small stresses during phase transformations. *Proceedings of the Royal Society of London. Series A. Mathematical and Physical Sciences*, 283(1394):403–422, 1965.

K. Hackl and F. D. Fischer. On the relation between the principle of maximum dissipation and inelastic evolution given by dissipation potentials. *Proceedings of the Royal Society A: Mathematical, Physical and Engineering Science*, 464(2089):117–132, 2008.

K. Hackl and R. Heinen. A micromechanical model for pre-textured polycrystalline shape-memory alloys including elastic anisotropy. *Continuum Mechanics and Thermodynamics*, 19(8):499–510, 2008.

K. Hackl, U. Hoppe, and D. M. Kochmann. Variational modeling of microstructures in plasticity. In *Plasticity and Beyond*, pages 65–129. Springer, 2014.

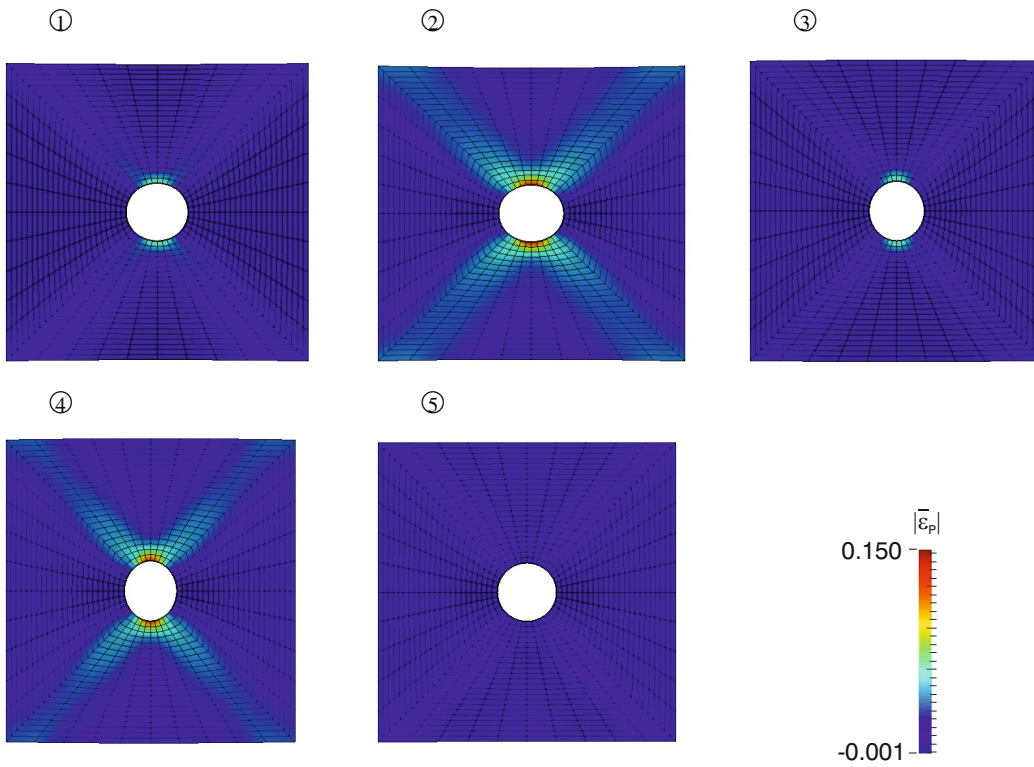


Fig. 6: Plate with a hole: norm of the plastic strain.

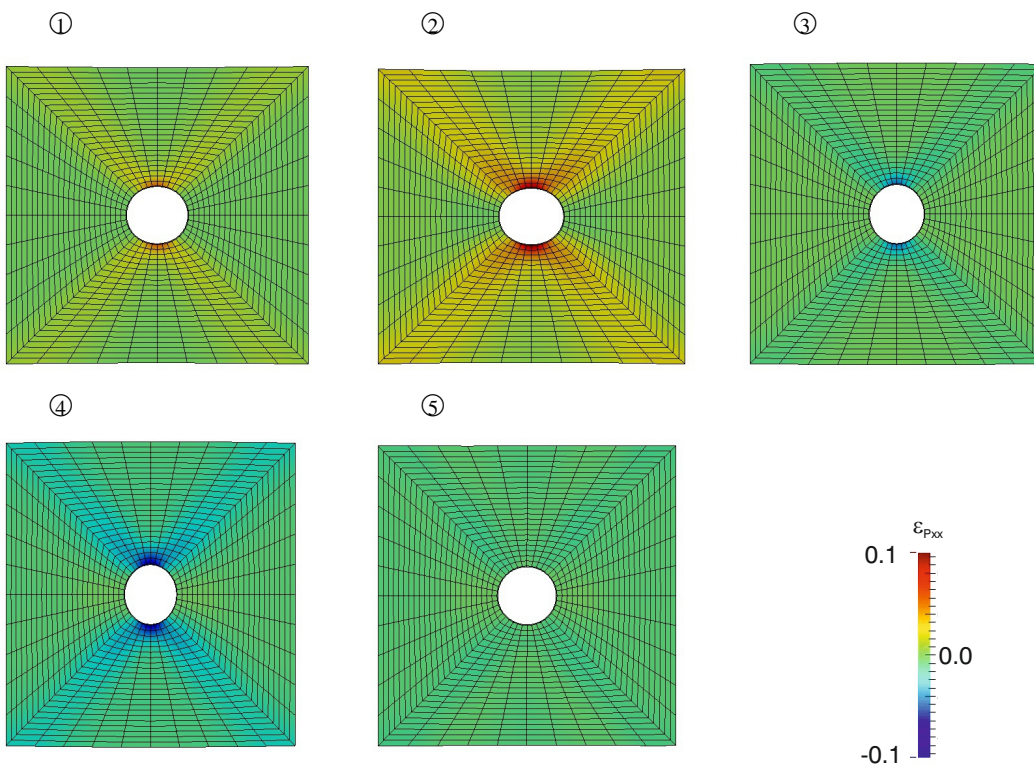


Fig. 7: Plate with a hole: xx -component of the plastic strain.

W. R. Hamilton. Xv. on a general method in dynamics; by which the study of the motions of all free systems of attracting or repelling points is reduced to the search and differentiation of one central relation, or characteristic function. *Philosophical transactions of the Royal Society of London*, (124):247–308, 1834.

W. R. Hamilton. Vii. second essay on a general method in dynamics. *Philosophical Transactions of the Royal Society of London*, (125):95–144, 1835.

W. Han, B. D. Reddy, and J. T. Oden. *Computational plasticity: the variational basis and numerical analysis*. 1995.

T. Iwamoto and T. Tsuta. Computational simulation of the dependence of the austenitic grain size on the deformation behavior of TRIP steels. *International Journal of Plasticity*, 16(7):791–804, 2000.

- T. Iwamoto and T. Tsuta. Computational simulation on deformation behavior of CT specimens of TRIP steel under mode I loading for evaluation of fracture toughness. *International Journal of Plasticity*, 18(11):1583–1606, 2002.
- P. Junker. An accurate, fast and stable material model for shape memory alloys. *Smart Materials and Structures*, 23(11):115010, 2014.
- P. Junker. Variational modeling of martensitic phase transformations. 2016.
- P. Junker and P. Hempel. Numerical study of the plasticity-induced stabilization effect on martensitic transformations in shape memory alloys. *Shape Memory and Superelasticity*, 3(4):422–430, 2017.
- J.-B. Leblond, G. Mottet, and J. C. Devaux. A theoretical and numerical approach to the plastic behaviour of steels during phase transformations—I. Derivation of general relations. *Journal of the Mechanics and Physics of Solids*, 34(4):395–409, 1986.
- J.-B. Leblond, J. Devaux, and J. C. Devaux. Mathematical modelling of transformation plasticity in steels I: case of ideal-plastic phases. *International journal of plasticity*, 5(6):551–572, 1989.
- V. I. Levitas. Thermomechanical theory of martensitic phase transformations in inelastic materials. *International Journal of Solids and Structures*, 35(9-10):889–940, 1998.
- J. Lubliner. A maximum-dissipation principle in generalized plasticity. *Acta Mechanica*, 52(3-4):225–237, 1984.
- J. Lubliner. *Plasticity theory*. Courier Corporation, 2008.
- H.-B. Mühlhaus and E. C. Alfantis. A variational principle for gradient plasticity. *International Journal of Solids and Structures*, 28(7):845–857, 1991.
- G. B. Olson and M. Cohen. Kinetics of strain-induced martensitic nucleation. *Metallurgical transactions A*, 6(4):791, 1975.
- R. Ostwald, T. Bartel, and A. Menzel. A one-dimensional computational model for the interaction of phase-transformations and plasticity. *The International Journal of Structural Changes in Solids*, 3(1):63–82, 2011.
- R. Ostwald, T. Bartel, and A. Menzel. Phase-transformations interacting with plasticity—A micro-sphere model applied to TRIP steel. *Computational Materials Science*, 64:12–16, 2012.
- A. S. J. Suiker and S. Turteltaub. Computational modelling of plasticity induced by martensitic phase transformations. *International journal for numerical methods in engineering*, 63(12):1655–1693, 2005.
- B. Svendsen and S. Bargmann. On the continuum thermodynamic rate variational formulation of models for extended crystal plasticity at large deformation. *Journal of the Mechanics and Physics of Solids*, 58(9):1253–1271, 2010.
- S. Thibaud, N. Boudeau, and J.-C. Gelin. TRIP steel: Plastic behaviour modelling and influence on functional behaviour. *Journal of materials processing technology*, 177(1):433–438, 2006.
- D. D. Tjahjanto, A. S. J. Suiker, S. Turteltaub, P. E. J. Rivera Diaz Del Castillo, and S. Van der Zwaag. Micromechanical predictions of TRIP steel behavior as a function of microstructural parameters. *Computational Materials Science*, 41(1):107–116, 2007.
- S. Turteltaub and A. S. J. Suiker. Grain size effects in multiphase steels assisted by transformation-induced plasticity. *International journal of solids and structures*, 43(24):7322–7336, 2006a.
- S. Turteltaub and A. S. J. Suiker. A multiscale thermomechanical model for cubic to tetragonal martensitic phase transformations. *International Journal of Solids and Structures*, 43(14-15):4509–4545, 2006b.
- J. Waimann, P. Junker, and K. Hackl. A variational material model for transformation-induced plasticity in polycrystalline steels. *Journal of the Mechanical Behavior of Materials*, 24(5-6):153–159, 2015.
- J. Waimann, P. Junker, and K. Hackl. A coupled dissipation functional for modeling the functional fatigue in polycrystalline shape memory alloys. *European Journal of Mechanics-A/Solids*, 55:110–121, 2016.
- J. Waimann, K. Hackl, and P. Junker. Variational modeling and finite-element simulation of functional fatigue in polycrystalline shape memory alloys. *Journal of Optimization Theory and Applications*, pages 1–27, 2019.
- P. Wriggers. *Nonlinear finite element methods*. Springer Science & Business Media, 2008.